Active touch remaps barrel cortex output from a representation of self-motion to object location.

Jonathan Cheung[1,2], Phillip Maire[1,2], Jinho Kim[1], Kiana Lee[1], Garrett Flynn[1], Samuel Andrew Hires[1*]

[1]Department of Biological Sciences, Section of Neurobiology, University of Southern California, Los Angeles, CA 90089, USA
[2]Neuroscience Graduate Program, University of Southern California, Los Angeles, CA 90089, USA
*Correspondence: shires@usc.edu

Abstract:
During active tactile exploration, the dynamic patterns of touch are transduced to electrical signals and transformed by the brain into a mental representation of the object under investigation. This transformation from sensation to perception is thought to be a major function of the mammalian cortex. In primary somatosensory cortex (S1) of mice, Layer 5B pyramidal neurons are the main outputs to downstream areas that influence perception, decision-making, and motor control. We investigated self-motion and touch representations in L5B of S1 with juxtacellular loose-seal patch recordings of optogenetically identified excitatory neurons. We found that during rhythmic whisker movement, 66% of neurons represent self-motion. This population was significantly more modulated by whisker angle than by phase. Upon active touch, a distinct pattern of activity was evoked across L5B, which represented the whisker angle at the time of touch. Object location was decodable with submillimeter precision from the touch-evoked spike counts of a randomly sampled handful of these neurons. These representations of whisker angle during self-motion and touch were independent, both in the selection of which neurons were active, and in the angle-tuning preference of co-active neurons. Thus, active touch transiently remaps the output of S1 from a representation of self-motion to explored object location.

Introduction:

A major function of the mammalian cortex is to integrate sensory input with self-knowledge to form mental representations of the external world to guide flexible behavior (Francis and Wonham 1976, Wolpert et al., 1995). Object location is one such representation, and it is essential for skillful navigation and object interaction (Vincent 1912, Sofroniew et al., 2015, Hoydal et al., 2019). Object locations can be rapidly and accurately identified via active touch (Lederman and Klatzky 1987, Knutsen et al., 2006, Mehta et al., 2007, Horev et al., 2011, Cheung et al., 2019). In active touch, mechanosensory input is thought to be referenced to the movement and position of tactile sensors to produce a mental percept not of the self, but of the object under investigation (Wolpert et al., 1995). Determining where and how these sensory and motor signals are transformed by neural circuits into a representation of the external world would improve our understanding of brain function.

Head-fixed mice are an excellent model system to investigate the neural basis of object localization. They can locate objects along the anteroposterior axis of the face with submillimeter precision by sweeping a single whisker back and forth (*i.e.* whisking; Cheung et al., 2019) and interpreting the mechanically-evoked neural activity patterns transduced in the follicle which holds the whisker (Li et al., 2011; Severson et al., 2017; Furuta et al., 2020). Similar sensorimotor mechanisms may underlie texture discrimination in rodents (Jadhav et al., 2009, Isett et al., 2018, Zuo et al., 2019a) and tactile sensing with tools in humans (Chan & Turvey 1991; Miller et al., 2019). High-speed whisker imaging and mechanical models of whisker deformation provide rich knowledge of the sensory input and motor program underlying the computation of object location (Kuntsen et al., 2008; Clack et al., 2012, Hires et al., 2013, Pammer et al., 2013, Hires et al., 2016, Vaxenburg et al., 2018). Early cortical processing of tactile input is topographically organized into columns of primary somatosensory cortex (S1) that have a one-to-one correspondence with large facial whiskers (Woolsey and Van der Loos 1970). Intrinsic signal imaging allows whisker-specific neural activity to be targeted for electrical recording (Masino et al., 1993; O'Connor et al., 2010). Furthermore, transgenic mouse lines allow assignment of observed neural activity patterns to neurons of specific types (Aranoff and Petersen 2008, Gerfen et al., 2013). Thus, mice allow a dissection of self-motion and object location representation at behavioral, perceptual, computational, and neural circuit levels.

A prime candidate for the construction of neural representations of object location are layer 5B (L5B) pyramidal neurons of S1. S1 activity is required for whisker-based anteroposterior object localization (O'Connor et al., 2010) (though not object detection; Hong et al., 2018). L5B pyramids are the major output of S1 to cortical and subcortical targets involved in decision making, action selection, and motor control (Lévesque et al., 1996, Kita and Kita 2012, Shepherd 2013; Gerfen et al., 2013). Distinct cellular compartments of L5B pyramids receive sensorimotor features that are assembled in models of object location representation and perception (Kleinfeld & Deschenes 2011; Cheung et al., 2019). These features include sensory representations of self-motion from ventral posteromedial nucleus of the thalamus (VPM) (Armstrong-James, et al., 1992; Fee et al., 1997; Petreanu et al., 2009), of touch from VPM and Layer 3 and 4 (L3, L4) of S1 (de Kock et al., 2007; Petreanu et al., Hires et al., 2015), and efference copy from primary motor cortex (M1) (Hill et al., 2011; Petreanu et al., 2012). Object location-specific calcium responses have been observed in tuft dendrites (Xu et al., 2012), apical trunk, and soma (Ranganathan et al., 2018) of L5B pyramids. Thus, L5B pyramidal neurons have the appropriate inputs and outputs to transform sensation into an object location representation that guides flexible behavior.

Here, we use single-unit juxtacellular electrophysiology to investigate the neural representation of sensory input, self-motion, and object location in L5B excitatory neurons during behavior. Over half of the active neurons encode self-motion during free-whisking, while a third encode the location of touched objects. This encoding does not require specialized training. Population responses to touch can decode object location with sub-millimeter accuracy. Contrary to expectations, the cellular identity and positional preferences of the touch-

evoked object location representation were uncorrelated with the self-motion representation during free-whisking. Thus, touch remaps rather than amplifies the neural representation of self-motion in L5B. These data suggest that a perceptual transformation from self to sensed object is accomplished by neural circuits interacting with L5B pyramidal neurons of S1.

Results:

Experimental design

To investigate the organization of neural representations in L5B during whisker-mediated exploration, we used variations of a go/no-go whisker-guided object localization task in head-fixed mice (O'Connor et al., 2010). Water-restricted mice (n=16 Vgat-ChR2-EYFP) were trained to whisk and contact a smooth vertical pole presented randomly across a contiguous range (10 mm) of pole positions along the anteroposterior axis about 8mm lateral from the whisker pad (**Figure 1A**). Mice were trimmed to a single whisker (C2) across all training and recording sessions. Whisker motion and object interactions were tracked from an overhead view at 1000 fps (**Figure 1B**). Whisker traces were converted to time series of whisker azimuthal angle (i.e. angle), the Hilbert decomposition of amplitude, midpoint and phase (Curtis & Kleinfeld, 2009) and touch (**Figure 1D**). We serially recorded optogenetically tagged single neurons via blind juxtacellular loose-seal patch in and around L5B of the C2 whisker representation of S1 (**Figures 1D, S1A and S1B; Methods**). Each trial consisted of a 0.5 s pre-pole period, followed by a 0.75 s stimulus sampling period, and then a 1.25 s answer period where licks triggered water dispensing or a brief time out (**Figure 1E**). We recorded from 156 single units during active touch behavior. Twenty units were silent and 14 others were putative inhibitory neurons, based on short latency spiking in response to illumination of S1 with 473nm light (**Figure S1C**), leaving 122 active excitatory neurons. To quantify the neural representation of sensorimotor features, we correlated these features to the times of detected action potentials.

Representation of self-motion

We first examined the neural representation of self-motion during free-whisking (**Figure S2A**). Most neurons (96 of 122 active units) were significantly (Chi-squared test) modulated (positively or negatively) by whisking, with the mean firing rate significantly increased from 5.0 ± 5.6 spks/s (mean ± SD) during non-whisking to 6.0 ± 7.1 spks/s (mean ± SD) during whisking (**Figure 2A**). Whisking tuned neurons were relatively uniformly distributed across the recorded depth (**Figure S2B**). Since whisking was volitional (Cheung et al., 2019), we could not dictate the exploration time or range of the mouse (**Figures S2C and S2D**), but many neurons (60/122) were significantly modulated with respect to whisker angle within the chosen range of whisking (**Figures 2B and 2C**). Across the population, preferred angles spanned the range of whisking (**Figures 2C and S2E**). Most of these neurons (46/60) were also modulated by phase in the whisker cycle (**Figures 2B, 2D and S2F**) with representations tiling the phase space. Across the population of 122 active units, 46 were co-tuned to whisker phase and angle, 14 to angle only, 0 to phase only, and 62 to neither [SH1](**Figure 2E**). Among neurons tuned to at least one, the mean depth of modulation to angle was significantly greater than to phase [SH2](p = 8.9e-6, **Figure and 2G, Methods**). Greater modulation to angle was more correlated with greater modulation to whisking midpoint than to amplitude, phase or velocity (**Figures 2H and 2I**). The absolute modulation depth of midpoint was most similar to that of angle (**Figure 2J**). This suggests that midpoint-correlated inputs are important for constructing an angle-tuned representation, which is consistent the importance of midpoint in predicting choice during object localization (Cheung et al., 2019). These data show that during free-whisking, L5B excitatory neurons encode a representation self-motion that is more specific to whisker angle than phase of whisk cycle.

Representation of object location

We then examined sensorimotor representations in the same neurons during active touch. Of the active excitatory neurons, 54 out of 122 were excited by touch. Touch responses were temporally sharp with short latency (**Table 1, Figure S3A**). In 42 of the 54 touch neurons, the number of spikes evoked was dependent on the anterolateral position of the pole (**Figure 3A**). These touch location tuned neurons were concentrated between 690-890μm from pia (**Figure 3B**), roughly corresponding to Layer 5B (**Figure 1D**, Lefort et al., 2009). There was minimal shift in follicle position across numerous touches in a trial (**Figure S3B and S3C**). Touch location tuning was driven by a greater probability of spiking and a greater number spikes evoked per touch (**Figure S3D and S3E**). Across the tuned population, the preferred object location spanned the entire range of touched pole locations (**Figures 3C and 3D**). The mean half-max width response was 1.8 mm (~9.2° of azimuth) (**Figure 3E**). Thus, this subpopulation of L5B excitatory neurons form a distributed neural code for touched object location.

Touch location tuning did not require training in whisker-guided location discrimination. We performed recordings in two related tasks. In 92 naïve recording sessions with untrained mice (n=10), water rewards were given randomly on 50% of the trials, regardless of pole location, while in 30 trained sessions, trained mice (n=6) were first trained to discriminate go and nogo locations as in Cheung et al., 2019 (**Figures 4A and 4B**) with water only available in the posterior go range. Trained mice made significantly more touches with less time spent whisking than naïve mice (**Figure S4A**). However, there was no significant difference in the proportion of touch responsive units that were tuned to object location between naïve (n=26/35, 74.3 %) and trained (n=14/19, 73.7 %) (p = 1.0, Fisher's exact test; **Figure 4C**), though we did observe a larger proportion of touch responsive units in trained animals (**Figure S4B**). The width of the tuning was indistinguishable between the groups (**Figure 4D**) and the preferred locations spanned the full range of presented locations in both naïve and trained mice (**Figures 4E and 4F**).

To access location information from a distributed representation, downstream neurons must sample multiple members of the representing population. However, the number of possible inputs to a neuron is limited. Thus, we wondered how accurately the object location could be determined from varying numbers of randomly sampled object-location tuned neurons. We constructed a multinomial generalized linear model (GLM) to predict the location of the pole from the distribution of the number of spikes evoked by single touches (**Methods, Figure S3F**[SH3]). A linear classifier pooling the touch-evoked spike counts from 25 of our location neurons (the subset with $\geq$ 75 touches in $\geq$ 80% of binned pole positions) predicted the pole location to $\leq$ 0.5 mm distance from actual [SH4]on 60.5% ± 1.3% (mean ± S.D.[SH5]) of touches (**Figures 5A and 5B**).

Our prior work showed that expert mice discriminate location to $\leq$ 0.5 mm resolution in this task (Cheung et al., 2019). How many location tuned neurons are required to meet or exceed the psychometric performance of these expert mice? We constructed neurometric performance curves from the predicted object locations (**Figure 5C**). Random sampling from five or more location tuned neurons produced virtual performance that met or exceeded expert behavior (**Figure 5D, Methods**). This suggests that downstream neurons that sample from at least five location-tuned 5B neurons have access to a touch-by-touch object-location representation that meets or exceeds the behavioral performance of the mouse.

Active touch remaps, rather than amplifies self-motion tuning

Does touch amplify an underlying whisker angle representation during free whisking? Or, does touch evoke an object-location representation that is independent of the free-whisking representation? Multiple lines of evidence support the independent model. First, 50% of neurons were tuned to angle during free whisking, and 36% were tuned to angle during touch, but only 20% neurons were tuned to angle under both conditions (**Figure 6A**). Thus, tuning during free whisking is neither necessary nor sufficient to exhibit angle tuning during touch. Moreover, this co-tuned overlap is nearly identical to and expected overlap (18%) if the two representations were independently distributed across the population.

We compared angle tuned responses between free-whisking and touch in individual neurons using spike integration windows derived from each neuron's touch-evoked response (**Figure 6B and S5A**). Whisker angle at touch is tightly correlated with (**Figure S3B**), and a proxy for the object location in this analysis (**Figure S3C, Methods**). The average absolute modulation depth was 3.6x greater for touch (14.6 ± 1.7 Hz; mean ± SEM) than for whisking (4.04 ± 0.5 Hz; mean ± SEM) (**Figure 6C**). Note that since touch evoked responses tended to be much larger, many neurons with higher absolute modulation to touch than whisking were not significantly touch angle tuned ($p<0.01$ ANOVA across angle bins). The shapes of normalized angle-tuning curves in each neuron were uncorrelated between the two conditions, and not significantly different from a randomly shuffled population (**Figure 6D**). Finally, the angles of maximum response during free-whisking and at touch were also uncorrelated (**Figure 6E**). Repeating these analyses using phase instead of angle as the independent variable showed similar results (**Figure S6**). We conclude that rather than amplifying an underlying tuning to whisker angle during free-whisking, active touch remaps L5B population activity from a representation of self-motion to an independent representation of object location.

Discussion:

We quantified sensorimotor representations in L5B excitatory neurons during active whisker exploration and touch using juxtacellular electrophysiology (**Figure 1**). Most active neurons represented self-motion during free whisking (**Figure 2**), with greater modulation by whisker angle than whisking phase. A third of L5B excitatory neurons were highly modulated by touched object location (**Figure 3**). This location tuning did not require training (**Figure 4**). Pooling activity of five random location-tuned units discriminated object location with equal or better skill than expert mice (**Figure 5**), suggesting that neurons in downstream areas need only sample a handful of S1 outputs to access behaviorally relevant representations of object location. The representations of whisker angle and phase during free-whisking and at touch were uncorrelated at population and within-cell levels (**Figure 6 and S6**). Together these data indicate that active touch remaps S1 output from a sensory representation of self-motion to a perceptual representation of object location.

Limitations and advantages of the research

We note several limitations of our work. We targeted recordings to L5B (Lefort et al., 2009) using axial penetration distance from pia to estimate cell depth, but cell-types do not strictly respect layer boundaries and this depth estimate is only accurate to within ± 30 μm (O'Connor et al., 2010b). Due to recording across multiple days during behavior, we did not attempt to recover cell morphology by juxtacellular filling. Thus, we could not determine which recordings were from thin vs. thick-tufted L5 pyramids or their projection patterns. Use of projection specific L5 *cre*-lines (e.g. intertelencephalic (IT) vs pyramidal tract (PT); Gerfen et al., 2013) could parse this in future work. Finally, we did not establish a causal role for location coding neurons in driving perceptual choice during object localization. Recent developments in structured illumination and optogenetics (Pegard, et al., 2017; Marshel et al., 2019) may allow testing this in the future.

However, our approach also had several advantages over prior investigations of S1 activity during whisker-guided object localization (Curtis & Kleinfeld 2009; Ranganathan et al., 2018). Optogenetic tagging allowed us to identify excitatory vs. inhibitory units. Juxtacelluar loose-seal recording, considered a gold-standard for extracellular single unit isolation (de Kock et al., 2008), allowed us to sample activity with high accuracy and temporal fidelity, without bias from firing rate, avoid misassignment of synchronous touch-evoked spikes (Hires et al., 2015), and avoid false negative responses common in calcium imaging when scanning population sized fields of view (Huang et al., 2019). The high temporal resolution of electrophysiology allowed us to determine whisker angle and phase tuning during free-whisking (**Figure 2**) and its relationship to tuning at touch (**Figures 3 and 6**), which was not investigated in prior studies using calcium imaging (Xu et al., 2012; Ranganathan et al., 2018).

The transformation from self-motion to object-location representation

Our investigation yielded two major surprises. First, L5B excitatory neurons show greater modulation to whisker angle than to phase during free-whisking (**Figure 2**). This is surprising because prior work showed that the vast majority of rapidly touch excited neurons across layers of rat S1 were phase, not angle tuned during free-whisking (Curtis & Kleinfeld, 2009). This suggests that reafferent phase modulation (Fee et al., 1997) in input layers of S1 (e.g. L4; Hires et al., 2015; Yu et al., 2016) is combined with other whisker position information (e.g. efference copy from M1; Hill & Kleinfeld 2011; Kleinfeld & Deschenes 2011) to produce angle-specific tuning in S1 output during free whisking. Furthermore, the rarity of angle-specific tuning across other layers of S1 (Curtis & Kleinfeld, 2009) suggests this combination of positional information occurs in the output layer (L5B) rather than across multiple intermediate layers of S1.

The second surprise is that within L5B, the cellular identity of angle tuned neurons (**Figures 6A and 6C**) and their angle preferences (**Figures 6B and 6E**) were uncorrelated between free-whisking and at touch. The same was true for phase tuning (**Figure S6**). This is surprising, because prior work across layers of rat S1 showed that touch responses are highly amplified when they occur at the peak of free-whisking phase tuning and suppressed when occurring at non-preferred phases (Curtis & Kleinfeld 2009). Moreover, the preferred phase during free-whisking and at touch were tightly correlated (Curtis & Kleinfeld 2009). Our observation of uncorrelated tuning again suggests that, upon touch, additional sources of positional information are integrated in L5B S1 to construct a representation of touched object location that is independent of the self-motion representation during free-whisking.

How is this remapping from self-motion to object location representation accomplished? At least three mechanisms could play a role. First, touch-induced follicle stresses differ from those during free-whisking (Severson et al., 2017), so distinct patterns of mechanosensory transduction (Furuta et al., 2020) likely underlie at least part of remapped tuning. Second, touch and whisking are encoded by largely distinct populations in superficial layers (Peron et al., 2015) which project to L5B (Lefort et al., 2009; Hooks et al., 2011). Thus, touch recruits a new set of interlaminar S1 projections that influence L5B responses. Third, touch could enhance integration of distant inputs on L5B dendrites (Ranganathan et al., 2018) by transient changes in dendritic conductances (Larkum et al. 1999). M1 input is strongest in electrically distant tuft dendrites of L5 neurons (Petreanu et al., 2009). Thus, touch could transiently increase the influence of efference copy from M1 on L5B activity, further contributing to the remapped tuning. Determining the extent to which each of these possible mechanisms contribute to object location tuning in L5B of S1 may reveal more general principles for how the transformation from sensation to perception is accomplished by cortical circuits.

Acknowledgements:

This work was funded by NINDS R01NS102808 and the Whitehall Foundation 2015-05-66.

Author Contributions:

Conceptualization, J.C. and S.A.H.; Methodology, J.C., P.M., J.K. and S.A.H., Software J.C., P.M. and S.A.H., Data curation, J.C., P.M., K.L., G.F., Investigation J.C. and P.M., Writing – Original Draft, J.C. and S.A.H., Writing – Review & Editing, J.C. and S.A.H., Funding Acquisition, S.A.H., Supervision, J.C. and S.A.H.

Declaration of Interests:

The authors declare no competing interests.

Figure Titles and Legends

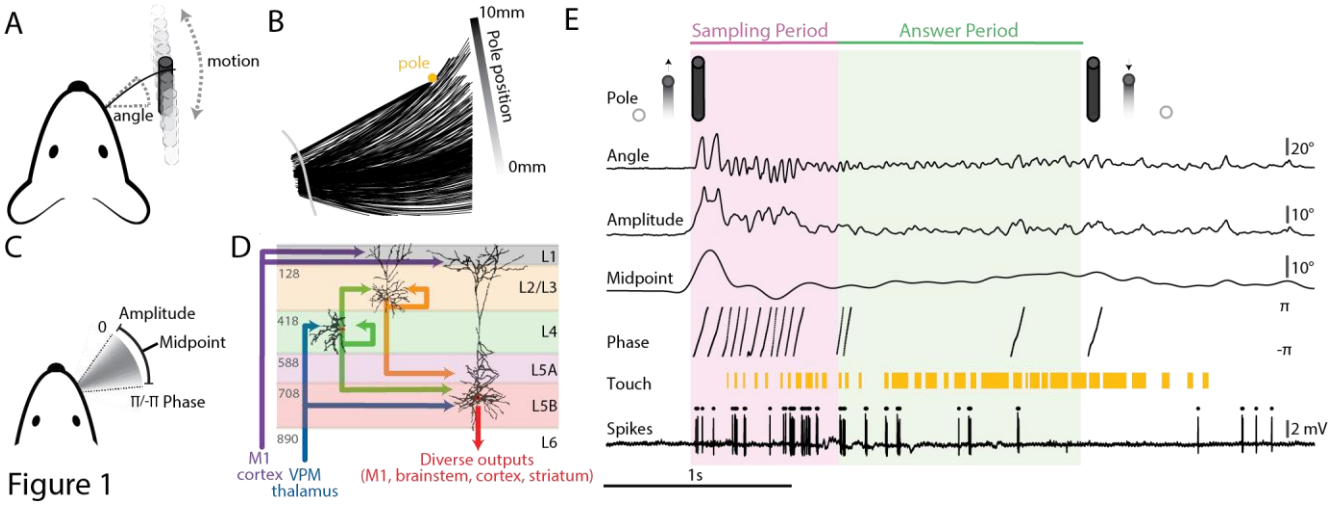

Figure 1 Head-fixed task and *in-vivo* juxtacellular electrophysiology

A) Schematic of task. Mice sweep a whisker forward and backward to locate a pole (black cylinder) presented along the anteroposterior axis. Angle is the azimuthal angle of the whisker at the follicle relative to the mediolateral axis of the animal. B) Overhead view of whisker traces captured from a single trial. A mask (gray) crops traces near fur. C) Angle time series can be decomposed to the Hilbert components amplitude, midpoint, and phase. D) Selected excitatory flow into L5B neurons of S1 (border depth in µm and dendritic arbors from Lefort et al., 2009). E) Trial structure with example traces of recorded stimuli and spikes. Phase masked to periods of amplitude > 5. Pole presentation is triggered 500 ms from trial start and takes ~200 ms to come into reach. Pole exits at varying times based on trial events.

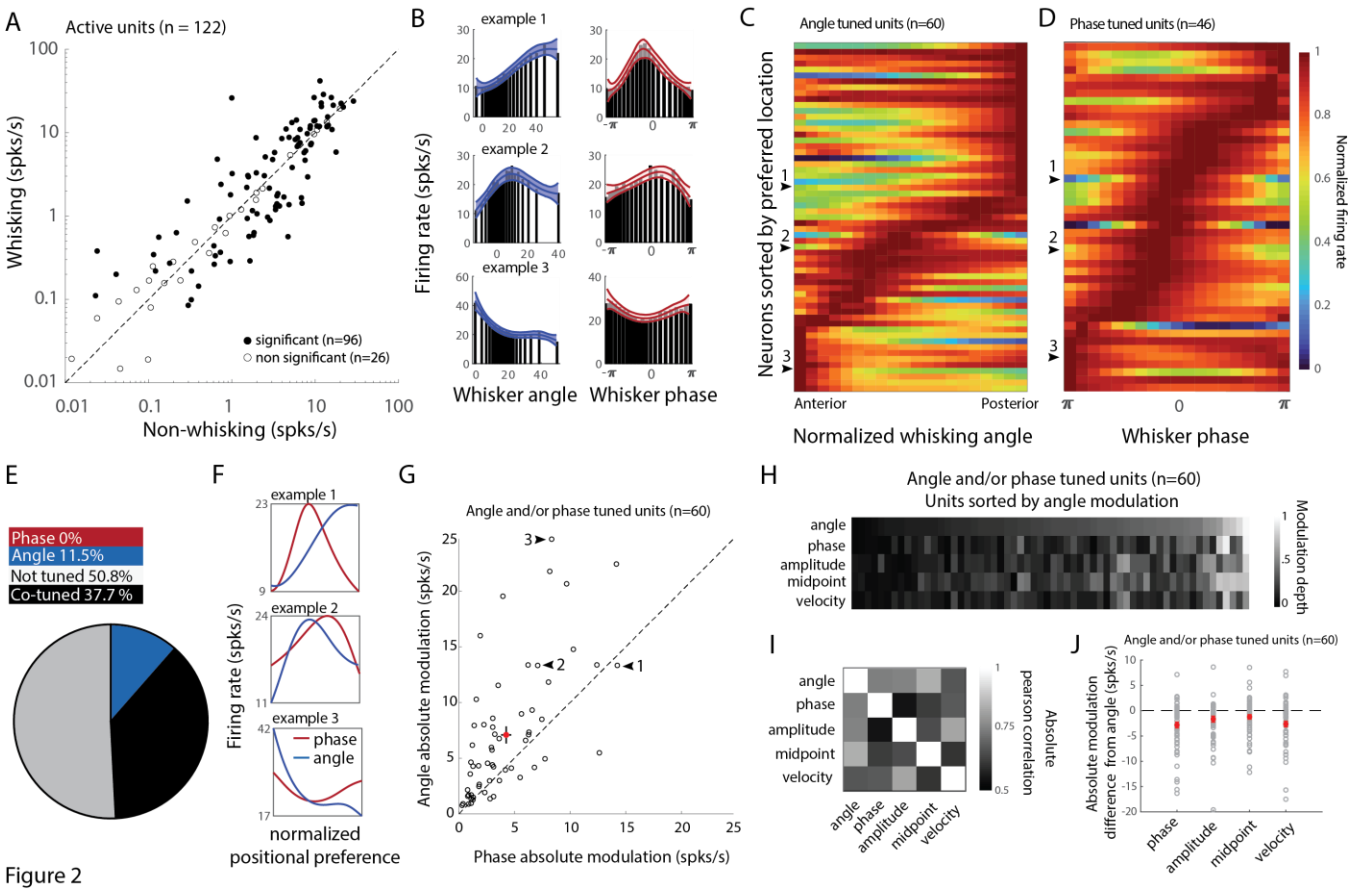

Figure 2

Figure 2 L5B excitatory neurons encode a representation of self-motion during free-whisking

A) Firing rates for non-whisking (5.0 ± 5.6 Hz) and whisking periods (6.0 ± 7.1 Hz) (p=2.9e-2, t-stat 2.2, df 121, paired sample t-test). Data are represented as mean ± S.D. B) Three example units tuned to both whisking angle (blue) and phase (red). C) Population heat map for units tuned to whisker angle sorted by peak angle response. D) Population heat map of phase tuned units sorted by peak phase response. E) Pie chart of self-motion tuning across the L5B excitatory population. Phase (red, 0/122), angle (blue, 14/122), co-tuned (black, 46/122) and not tuned to either (gray, 62/122). F) Normalized positional preference for the 3 examples in B, phase (red), angle (blue). G) Absolute modulation depth (**Methods**) comparison between free-whisking phase and angle tuning. Red dot and error bars denote phase/angle mean ± SEM (4.2/7.1 ± 0.5/0.8 spks/s, p = 8.88e-6, t-stat= -4.87, df = 59; paired t-test). H) Modulation depth of angle, phase, amplitude, and midpoint for all angle tuned units. I) Contingency table of Pearson correlation coefficients for modulation depths across angle and motor variables. J) Difference in absolute modulation between angle and motor variables (motor – angle modulation). Phase to angle (mean ± SEM = 2.8 ± 0.6, p = 8.9e-6, *t*-stat = 4.9, df = 59). Amplitude to angle (mean ± SEM = 1.7 ± 0.6, p = 8.2e-3, *t*-stat = 2.7, df = 59). Midpoint to angle (mean ± SEM = 1.2 ± 0.5, p = 0.01, *t*-stat = 2.7, df = 59). Velocity to angle (mean ± SEM = 2.6 ± 0.6, p = 2.4e-5, *t*-stat = 4.6, df = 59). All compared using paired t-test.

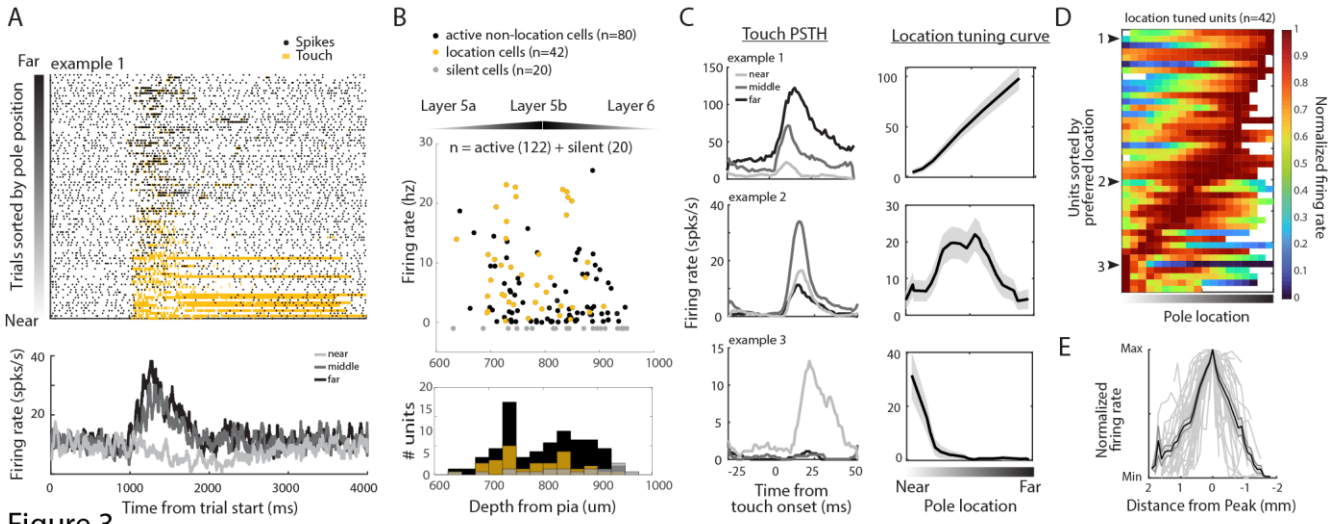

Figure 3

Figure 3 L5B S1 excitatory units are tuned object location at touch.

A) Raster for example neuron (top) tuned to far object locations (bottom). B) Average firing rate vs. depth from pia for active non-location (black), location (gold), and silent (gray) units. C) Touch peri-stimulus time histogram (left) and location tuning curves (right) for three example units tuned to far (top), middle (middle), and close (bottom) pole positions. Data are represented as mean ± SEM. D) Population heat map of object-location tuned units, sorted by preferred location. White spaces are insufficiently sampled pole locations. E) Shape of normalized tuning curves across all object-location tuned units. Data are represented as mean ± SEM. Mean half-max width response was 1.8 mm (~9.2° of azimuth).

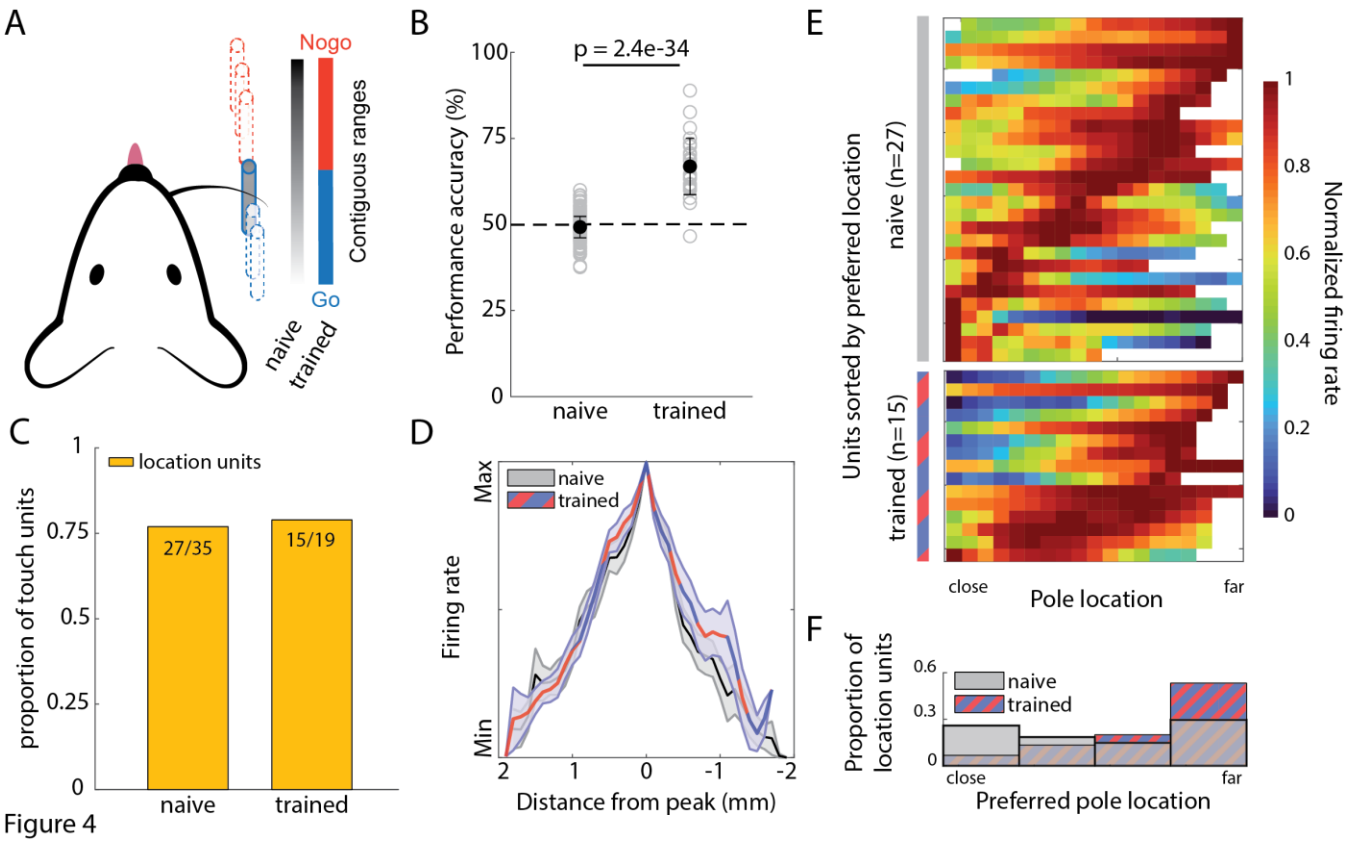

Figure 4

Figure 4 Object location tuning does not require specialized training.

A) Schematic of two tasks. Mice were presented a pole randomly in a 10mm range, 7 – 12mm from the face. Naïve task, reward was available on 50% of trials, regardless of pole position. Trained task, reward exclusively available 100% of time in 0-5mm proximal Go range. B) Performance on naïve (49.3% ± 3.1% mean ± SD) and trained (66.9% ± 8.1% mean ± SD) recording sessions (p = 2.4e-34, t-stat = 17.2, df = 120, unpaired *t*-test). C) Proportion of touch units that are location tuned for naïve (left; 77.1%) vs trained (right; 78.9%) animals. D) Shape of normalized tuning curves for touch location units from naïve (gray) and trained (red/blue) mice. E) Population heatmap of touch location units from naïve (top 27 units) and trained (bottom 15 units) animals, sorted by preferred object location. Each row denotes a single location neuron. F) Histogram of positional preference of touch location units compared between naïve and trained animals. (p=0.12, *t*-stat = -1.6, df = 40; two-sample *t*-test)

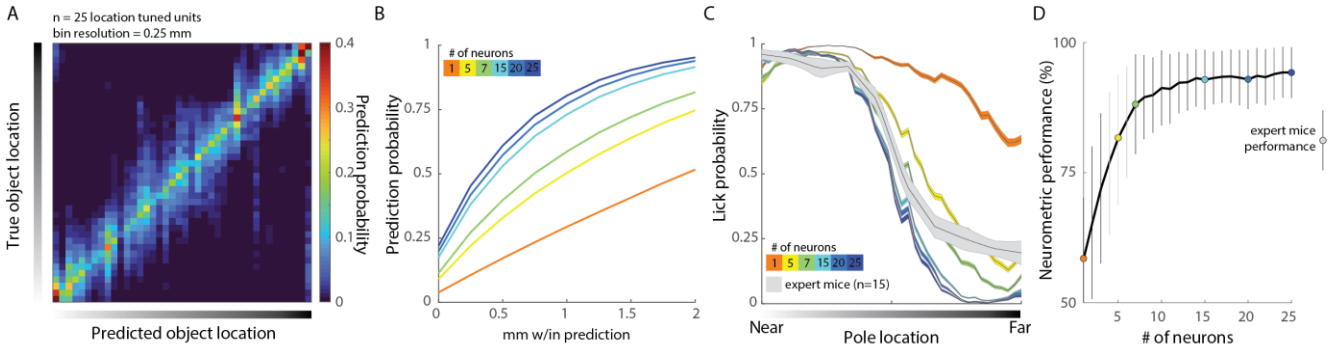

Figure 5

Figure 5 Object location is decodable to <0.5 mm precision from touch-evoked spike counts.

A) Contingency table of pole location decoding performance from 25 pooled unique touch location units using a multinomial GLM B) Performance as a function of pool neuron count. C) Average psychometric curves from 15 expert mice (gray; Cheung et al., 2019) and neurometric curves from varying numbers of sampled location units. D) Performance from neurometric curves compared to expert mice. Data are represented as mean ± S.D. Solid black lines denote points significantly different ($p < 0.05$; two-sample *t*-test) from expert mouse performance.

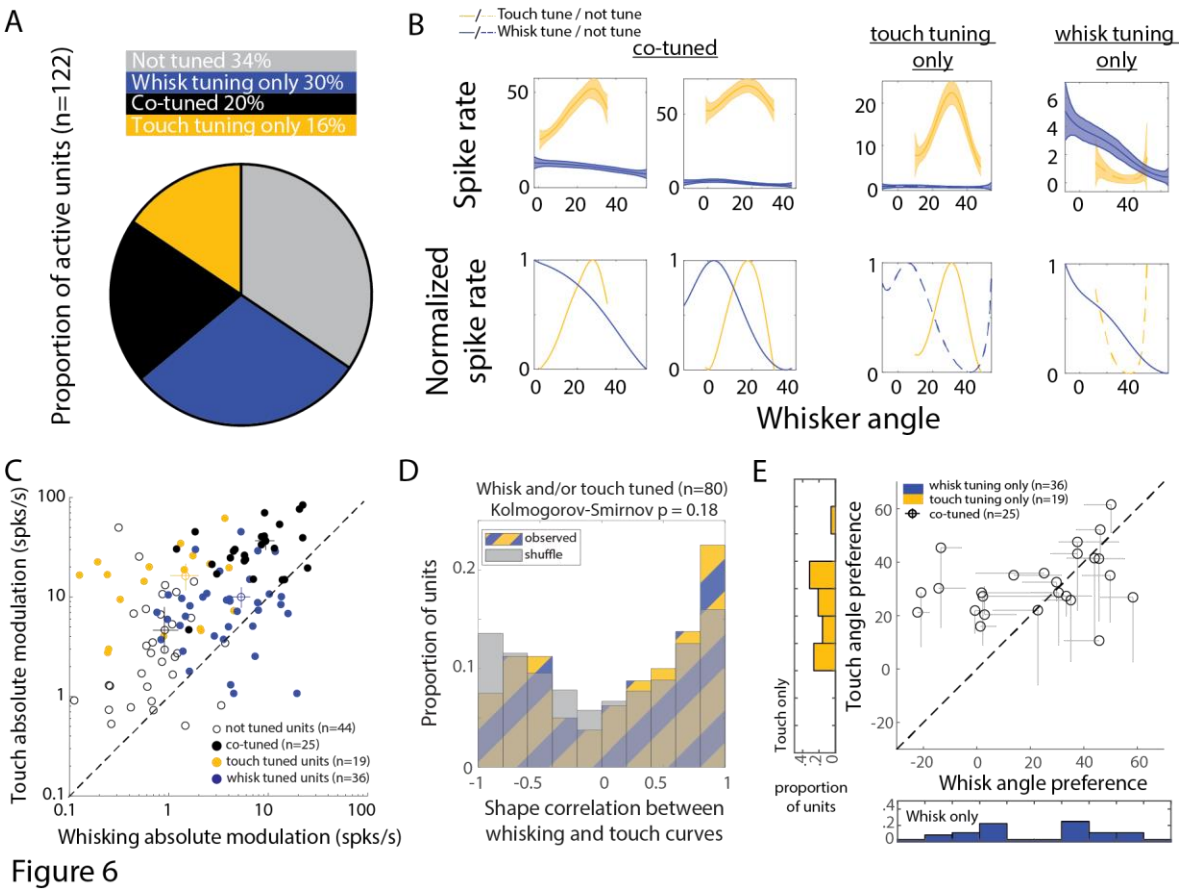

Figure 6

Figure 6 Active touch unmasks a distinct population code for object position in Layer 5 of S1.

A) Proportion of units tuned to whisker angle during free-whisking (blue, 36/122), at touch (gold, 19/122), co-tuned (black, 25/122), or not-tuned (gray, 44/122). B) Absolute (top) and normalized (bottom) tuning curves for angle responses during free whisking (blue) and at touch (gold). C) Absolute modulation depth for angle tuning during free-whisking and touch for each class in A. D) Shape correlation between whisking and touch tuning curves for all units tuned to whisking and/or touch (blue and gold hash) compared to shuffled responses (gray). Kolmogorov-Smirnov p=0.18. E) Preferred angle during free-whisking vs. at touch. Single-tuned units on histograms, co-tuned units on plot. Distance from midline for co-tuned units: (mean ± SD = 12.6 ± 10.9°, p = 9.7e-6, *t*-stat = 5.6, df = 24; one sample t-test)

	Non-touch units (n=68)				Non-location touch units (n=12)				Location touch units (n=42)			
	Mean	SD	Median	min - max	Mean	SD	Median	min - max	Mean	SD	Median	min - max
Whisking (Hz)	4.47	5.81	1.38	.01 - 23.86	4.14	4.33	2.67	.20 - 26.33	9.10	10.20	5.44	.06 - 41.70
Quiet (Hz)	4.27	5.26	2.15	.04 - 43.89	3.79	4.38	1.53	.10 - 29.05	6.65	6.37	4.41	.04 - 28.81
Proportion of spikes evoked by touch	0.19	0.17	0.13	.00 - .72	0.33	0.23	0.26	.05 - .72	0.41	0.23	0.33	.09 - .99
Proportion of spikes evoked by touch + whisking	0.45	0.19	0.42	.10 - .88	0.52	0.21	0.56	.18 - .86	0.60	0.20	0.60	.16 - .99
Touch onset latency (ms)					12.33	6.33	11.00	6.00 - 26.00	10.12	4.39	9.50	4.00 - 22.00
Touch response duration (ms)					17.25	8.84	16.00	4.00 - 34.00	18.52	9.75	17.50	4.00 - 43.00
Spikes in response window (#)					0.40	0.33	0.37	.04 - 1.25	0.74	0.80	0.52	.07 - 3.60
Probability of touch response					0.29	0.19	0.26	.03 - .64	0.43	0.29	0.43	.05 - .93
Probability of response at peak bin					0.36	0.19	0.33	.07 - .84	0.55	0.27	0.59	.09 - .99
Probability of response at trough bin					0.21	0.23	0.12	.00 - .65	0.26	0.24	0.18	.00 - .88
Response at peak bin (Hz)					24.97	10.32	22.44	48.37 - 233.33	51.87	35.49	42.15	45.45 - 200.00
Response at trough bin (Hz)					11.58	10.47	6.99	45.88 - 200.00	19.97	21.60	13.79	27.00 - 200.00

Table 1: Table comparing properties of non-touch (n=68), non-location touch units (n=12), and location touch units (n=42).

MATERIALS AND METHODS

LEAD CONTACT AND MATERIALS AVAILABILITY

Further information and requests for resources and reagents should be directed to and will be fulfilled by the Lead Contact, Samuel Andrew Hires (shires@usc.edu).

EXPERIMENTAL MODEL AND SUBJECT DETAILS

Sixteen VGAT/ChR2/EYFP mice (JAX B6.Cg-Tg), both male and female, of at least 3 months of age were used for the following experiments. A complete description of the head-plate procedure has been documented in previous work (Guo et al., 2014). Post-op, mice were housed with littermates or singly housed if fighting occurred. Mice were provided food *ad libitum* and water restricted to 1 mL per day for one week before training and recording. A daily health and weight assessment was completed to ensure mice were healthy. All procedures were approved under USC IACUC protocols 20169 and 20731.

METHOD DETAILS

- *Object localization task*

Mice were trained in a whisker based go/no-go object localization task. Using a single whisker (C2), water-restricted mice were motivated to whisk and identify the location of a smooth vertical pole (0.6mm diameter) 7-12mm lateral from the whisker pad. The pole moved along the anteroposterior axis acoss 10 mm was positioned using stepper linear actuators with 99 nm resolution, 25 µm accuracy and <5 µm repeatability (Zaber NA11B30-T4). To avoid potential ultrasonic cues associated with stepper motor movement, the pole was jittered 0-127 microsteps (0-25 µm) on each trial. A pneumatic linear slider (Festo) was used to raise the pole vertically into touch reach for each trial. The Festo also provided a sound cue on pole presentation onset.

Specific pole locations rewarded mice with water (4-8 µL), punished mice with a timeout (2 s), or had no effect based on the mouse's decision to lick or withhold licking. In a go/no-go paradigm, four trial outcomes exists. In a minority of sessions where the animals were trained, the close posterior 5 mm of pole positions (go) were rewarded with water rewards upon licking (hit) or had no effect if mice withheld licking (miss). The far anterior 5mm of pole positions (no-go) were punished with timeout (false alarm) or had no effect if mice withheld licking (correct rejection). For the remaining sessions, rewards and punishment were given regardless of the pole location - go trials and no-go trials had overlapping pole locations.

- *Behavior, videography, and electrophysiology*

Animal behavior, videography and electrophysiology were synchronized and captured during task performance using EPHUS (https://www.janelia.org/open-science/ephus). A single computer running BControl (MATLAB 2007b) was used to initiate each trial of the object localization task and synchronize video and electrophysiology recordings via a second computer running EPHUS. Trial onset triggered high-speed video capture of whisker motion (1000 fps) and electrophysiology recording of single unit activity (MultiClamp 700b).

Whisker motion was captured from an overhead view and spanned 4 seconds, spanning the period prior to pole onset to response window. Video frames were acquired using Basler acA200-340kmNIR camera and Edmund Optics 0.18X 1⁄2'' GoldTL Telecentric Lens (Model # 52-258) under 940 nm illumination on Streampix 6 software. Whisker shape and position was traced and tracked using Janelia Farm's Whisker Tracker (https://www.janelia.org/open-science/whisk-whisker-tracking). A mask was traced around the edge of the fur to reduce tracking noise. Whisker angle is quantified as the intersection between the mask and the whisker. The

whisker midpoint, phase and amplitude was decomposed from the band-pass filtered (6-60 Hz, Butterworth) whisker angle time series using the Hilbert Transform (MATLAB 2018b: *hilbert*). Whisking amplitude and phase is defined as the magnitude and phase angle (radians) of the Hilbert Transform of the whisker angle time series, respectively. Whisking midpoint is the filtered (6-60 Hz) difference between whisker angle time series and band-pass filtered signal. Whisker curvature is the amount of bending of the whisker measured 3-5 mm lateral from the whisker mask.

The precise millisecond of touch was determined through custom MATLAB software via distance to pole and change in whisker curvature. This was followed with manual curation of images of uncertain whisker and pole intersections.

- *In-vivo loose seal juxtacellular recordings*

All animals used in this study were adult male or female transgenic mice (VGAT-ChR2-EYFP) expressing channelrhodopsin in inhibitory units. Following head-plate surgery, mice were trimmed to one whisker (C2) and intrinsic signal imaging was used to target the barrel column associated. A single whisker was maintained throughout training and recording. Prior to recording, animals were anesthetized (2% isofluorane) and a small craniotomy (200-300 µm) was made above the barrel column associated with the C2 whisker. On the first day of recording, animals were allowed to recover for 1 hour before recording. Recordings were repeated for 4.8 ± 1.5 sessions (mean ± SD) per animal.

To sample single unit spiking activity in a manner unbiased by firing rate, blind juxtacellular loose-seal patch recordings were targeted to L5 (600 µm - 950 µm from pia; Lefort et al., 2009) neurons using patch pipettes (Warner Instruments; 5-8 MΩ) filled with 0.9% saline (Growcells). Electrical recordings (n=156 neurons) were acquired and amplified using MultiClamp 700b and Headstage CV-7B. The pipette axis was aligned parallel to the C2 barrel column at 35°. To perform an unbiased sampling of L5B, we recorded from any isolated unit. An isolated unit was identified by an increase in resistance to 15-20 MΩ. Once a unit was isolated, 10 trials of the behavioral task was run to test for spikes during performance. If spikes were observed an isolated unit was maintained for at least 100 trials (137 ± 57; mean ± SD). Upon recording completion, 10 trials of a 10 Hz pulse of blue light (480nm, 10, 20ms at 15-20 milliwatts) was used to test whether the unit was an interneuron. Short latency spiking (or inhibition) to a 490nm 10 Hz 5ms light indicated if the neuron was inhibitory (or excitatory) (**Figure S1**). Fourteen units were inhibitory and excluded from analysis. On the other hand, if an isolated unit did not spike after 10 trials a current pulse (100 us, 20 nanoamps) was injected to check if a unit was indeed patched. If a burst of spikes was observed, we deemed that neuron a silent cell.

- *Histology*

DiI (ThermoFisher D282) was coated onto a patch pipette and inserted into the recording location on the final day of recording to identify the location of recordings. DiI coated pipettes were inserted 1000um deep into the recording location and left there for 5 minutes to ensure proper coating of the recording location. 2 hours post dye, animals were deeply anesthetized with ketamine (110mg/kg) – xylazine (10mg/kg) cocktail before perfusion with 0.1 M sodium phosphate buffer, followed by 4% paraformaldehyde (PFA, in 0.1M sodium phosphate buffer). The fixed brain was then flattened along the axis perpendicular to the barrel column.

The flattened brain was immersed in 4% PFA for 1 hour post-perfusion, transferred to 20% sucrose solution for 1 day, and then 30% sucrose for 1 day. 100 µm slices were cut tangentially and cytochrome oxidase staining was performed to reveal the barrel columns. Fluorescence imaging was done to recover the location of the DiI track. Recording location was determined by overlapping fluorescent track on top of bright field imaging of barrel columns.

QUANTIFICATION AND STATISTICAL ANALYSIS

- *Defining touch response window*

A smoothed (Bayesian Adaptive Regression Splines [BARS] Wallstrom et al., 2008) response -50 ms to 50 ms around touch was used to evaluate the touch response window. The touch response window is defined as any time point from 5 to 50 ms post-touch in the smoothed response that exceeded baseline (-50 to 0 ms pre-touch) ± the 95% confidence interval. 2 parameters were imposed to ensure an accurate response window was captured: 1) the mean firing rate of the touch response had to be > 2 Hz: 2) the touch response window had to be greater than 4 milliseconds. A touch neuron is defined as any neuron that had a touch response window.

- *Tuning curves*

For a single neuron 5% of sampled touches or 5% of total whisking time points were used to define a point along the touch or whisking tuning curve. This method ensured 20 equally sampled bins. Stimulus values are defined as the median of each stimulus bin and the response values as the mean of each response bin. For touch tuning the response bins include the firing rates within the touch response window as defined above. For whisking tuning the same response window as touch was used. If a neuron was not tuned to touch, the median touch response window was used to evaluate whisking tuning. The median touch response window is 10 to 28 milliseconds post-touch. Tuning curves were generated by smoothing using Bayesian Adaptive Regression Splines on the binned histograms. Neurons that had mean whisking responses less than 2 Hz were not evaluated.

We used a one-way analysis of variance (ANOVA) at alpha level of 0.01 to quantify whether a neuron was tuned or not to a whisking or touch parameter. To further ensure that the tuning we observed was not due to noise in neural responses, we shuffled touch/whisking responses 1000 times and evaluated F-values from a one-way ANOVA. If our observed F-value was above the 95th percentile of the shuffled population distribution of F-values we deemed the neuron as tuned.

Tuning preference is the location of the peak response of the tuning curve. To define the width of the tuning, a multiple comparison test using Tukey-Kramer type critical value was used to identify the first bins in both direction that were significantly different from the peak value. If no bins were significant, no modulation width was defined. Maximum and minimum responses were calculated from BARS fitted tuning curves.

In computing tuning curves whisker angle at touch instead of object location we find that two more units qualify as tuned (**Figure S3E and S5C**). Upon closer inspection we discover that those two units exhibit a non-linear 2nd order polynomial relationship between whisker angle and pole location. This second order polynomial fit leads to non-linear increases in whisker angles for incremental gains in pole location, causing those two units to have tuning to far locations not seen when observing pole locations.

- *Modulation*

The absolute modulation depth and modulation depth for each tuning curve is calculated as:

$$absolute\ modulation\ depth = \max response - \min response$$

$$modulation\ depth = \frac{\max\ response - \min response}{\max\ response + \min response}$$

- *Neural decoding*

We used multinomial logistic regression to decode pole location implemented using *glmnet*. (Qian et al., 2013). Only touch units that sampled at least 80% of the pole position range were used for decoding. Each unit had a tuning curve that was interpolated to 40 bins to estimate location to 0.25 mm resolution. At each bin, 50 samples were drawn from a Poisson pdf with a λ as the mean of each interpolated bin. We justified drawing from a poisson pdf because we found that at touch the number of spikes generated in the touch response window followed a Fano factor of 0.94 ± 0.22 (mean ± SD, **Figure S3F**). For the design matrix, each row is a location bin, each column a single neuron, and each entry a sampled neural response for the associated neuron.

The decoder was run for 10 iterations. During each iteration a random 70% of trials were allocated for training and the remaining 30% for test. Lasso regularization (alpha parameter 0.95) was used to reduce over-fitting. To identify the number of units required, we sampled varying numbers of neurons with replacement from the units used to train the original model 500 times. The indices of the selected neurons were used to create a new population design matrix and matrix of learned coefficients from the original design matrix and learned coefficients. The prediction probabilities of location were computed by the below:

$$h_\theta(x) = g(\theta^T x)$$

$$\text{where } g(z) = \frac{1}{1+e^{-z}}$$

where $h_\theta(x)$ is the hypothesis function, θ^T are the learned coefficients, x is the input design matrix, and $g(z)$ is the normal function of logistic regression used to calculate prediction probabilities.

The predicted location was chosen as the location with the highest probability. Model evaluation of accuracy and resolution was performed on the test set. Model accuracy is defined as the total number of correct predictions divided by the total number of predictions. A confusion matrix made from true and predicted locations was normalized across the total number of given true cases and used to define the decoding resolution and neurometric curves. Decoding resolution is defined as the total number of predictions within *n* bins of the diagonal, where each bin was 0.25 mm. Neurometric curves, defined here as the choice to lick given neural activity, is defined as the sum of predictions along true values for the go predictions (left half of the confusion matrix). Simulated neurometric curve performance for licks were defined as any lick probability that exceed 50%.

DATA AND CODE AVAILABILITY

Please contact the lead contact for data structures used in the analysis above. All analyses were computed in MATLAB 2018b and all code for generating figures can be found at (https://github.com/hireslab/Pub_LocationCode)

Supplementary figures

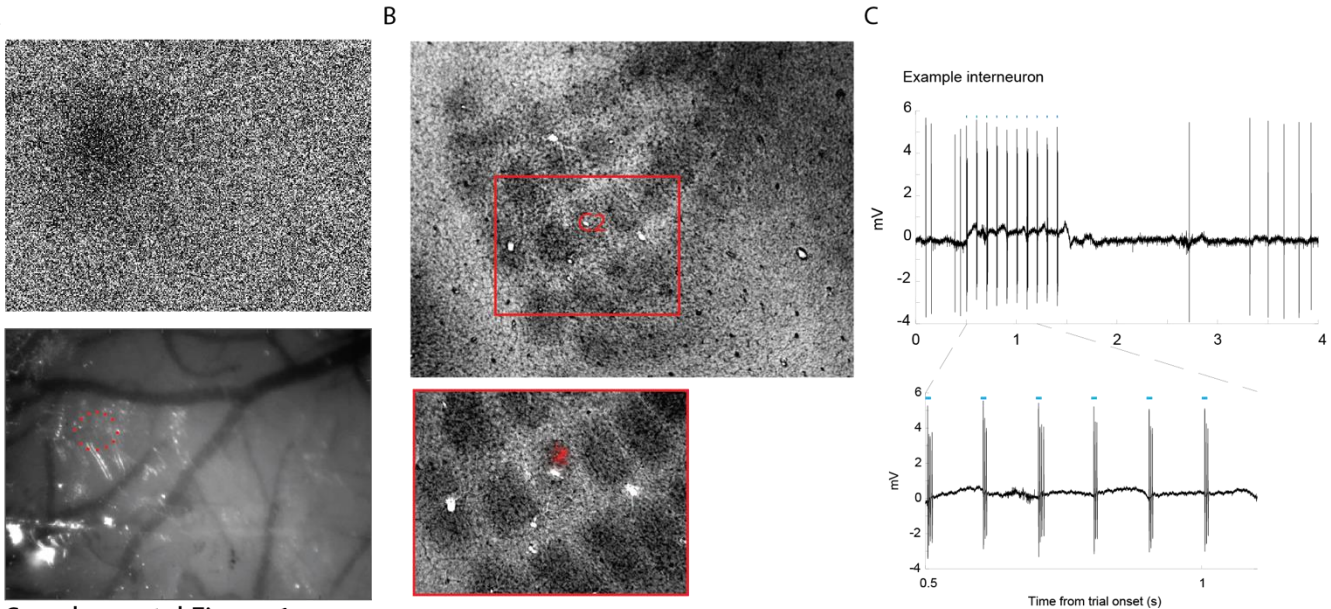

Supplemental Figure 1

Supplementary figure 1 Recording targeting, recovery, and opto-tagging.

A) Intrinsic signal imaging highlighting region of activity during whisker stimulation (top) overlaid with skull vasculature. B) 4x (top) and 10x (bottom) zoom of recovered DiI on top of cytochrome oxidase labeling of barrel field. C) Example trace of single stimulation (480nm 10Hz pulse) trial (top) with zoom of first 500 milliseconds of stimulation (bottom).

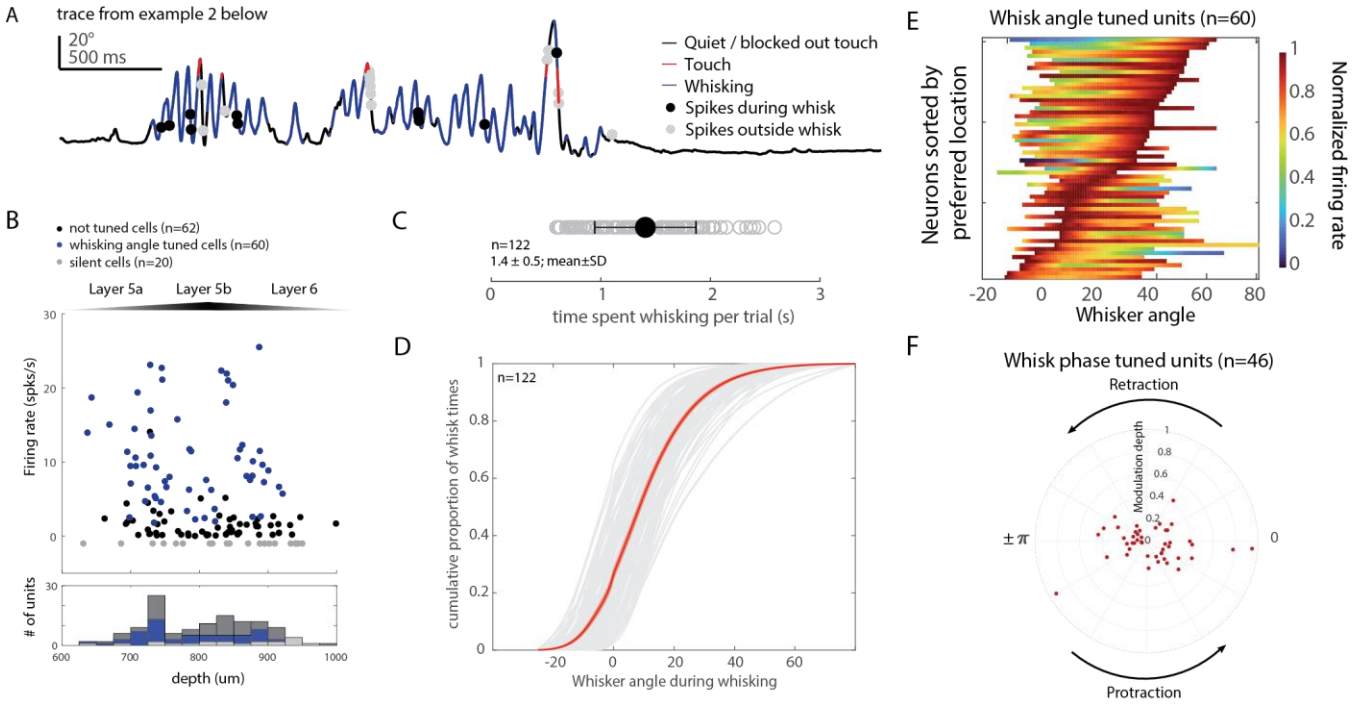

Supplemental Figure 2

Supplementary figure 2 Whisker angle during free-whisking tuning

A) Example whisker trace with spikes overlaid for one example cell tuned to whisker angle during free-whisking. B) Average firing rate and depth from pia for active non-location (black), whisking angle (blue), and silent (gray) units. C) Scatter of mean ± SD (1.4 ± 0.5) for time (seconds) spent whisking for each recorded neuron. D) Cumulative distribution function of whisker angle sampling during free whisking for all recorded units (gray) and population average ± SEM (red). E) Free-whisking angle tuning across the population of significantly tuned units (n=60). F) Phase preference with modulation depth (**Methods**) across the population of phase-tuned units (n=46).

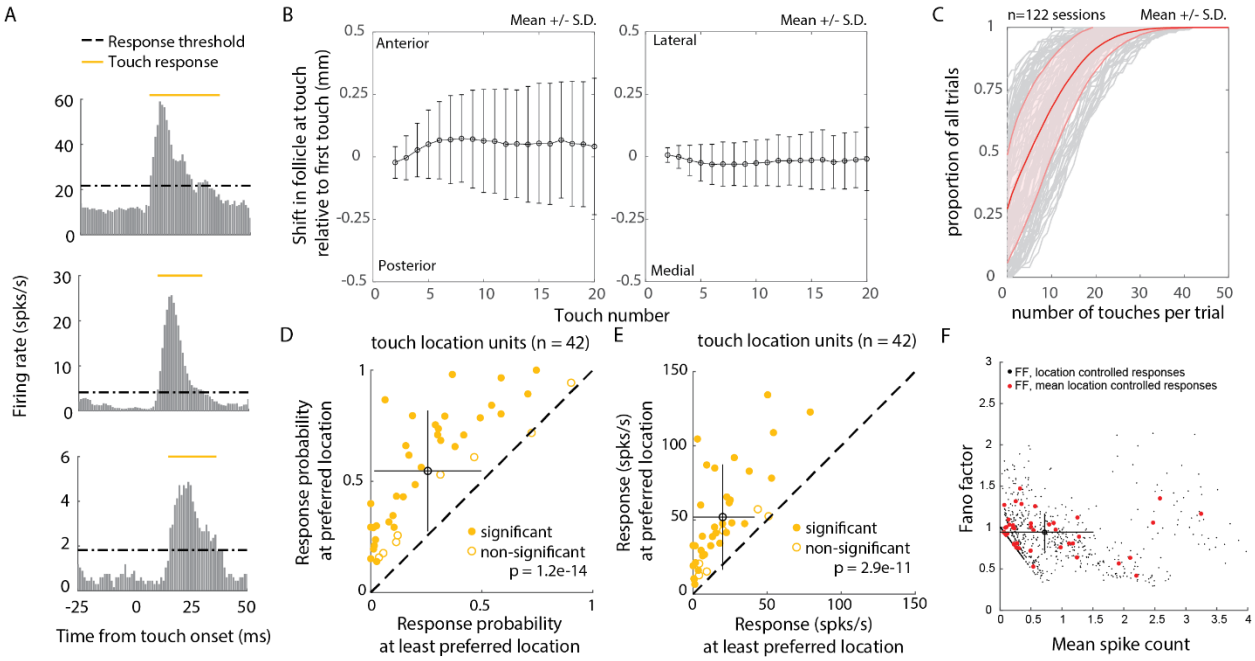

Supplemental Figure 3

Supplementary figure 3 Whisker angle during touch tuning

A) 3 example touch units and their responses from touch onset. B) The change in follicle relative to the first touch along the anteroposterior axis (left) and mediolateral axis (right). C) Cumulative distribution function showing the number of touches made for each recording session (gray, n=122) and the population average ± S.D. (red). D) Response probability of generating a response above baseline ± 95% CI in the most preferred location versus the least preferred location (p = 1.2e-14, *t*-stat = 11.7, df = 41, paired t-test). E) Same as D but for the firing rate of responses (p = 2.9e-11, *t*-stat = 8.9, df = 41, paired t-test). F) Justification for modeling spikes using a Poisson process. Black dots denote scatter of spike count (0.73 ± 0.81, mean ± SEM) against Fano factor (0.94 ± 0.24, mean ± SEM) for each point along the angle at touch tuning curve (n = 784 points). Red dots denote average for each individual location at touch tuned neuron.

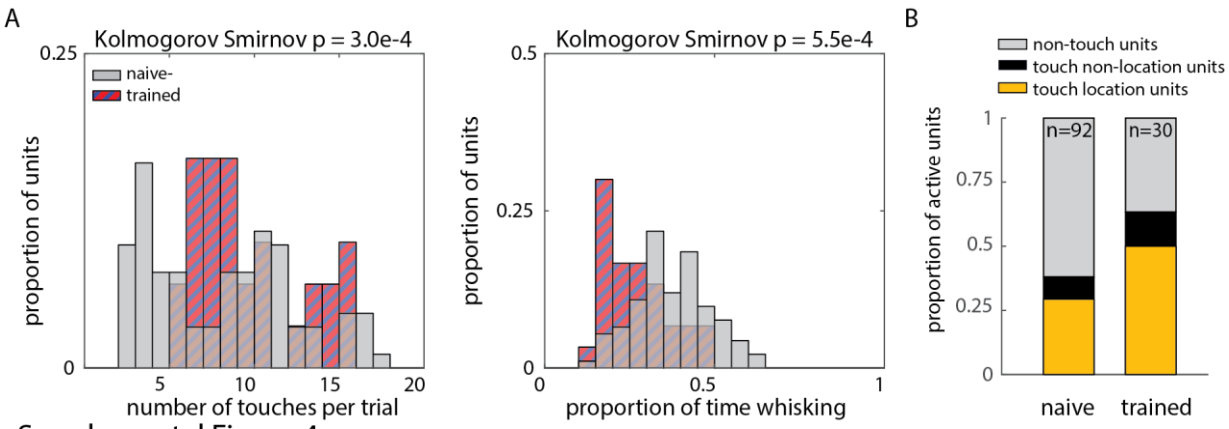

Supplemental Figure 4

Supplementary figure 4 Naïve vs trained animals comparison

A) Comparison of number of touches made per trial (left, p=3.0e-4) and proportion of time whisking (right, p = 5.5e-4) between naive (gray) and trained animals (red/blue hash). Both compared using two-sample Kolmogorov-Smirnov test. B) The distribution of non-touch units, touch location units, and touch non-location units compared between recordings from naïve (n=92) and trained (n=30) animals

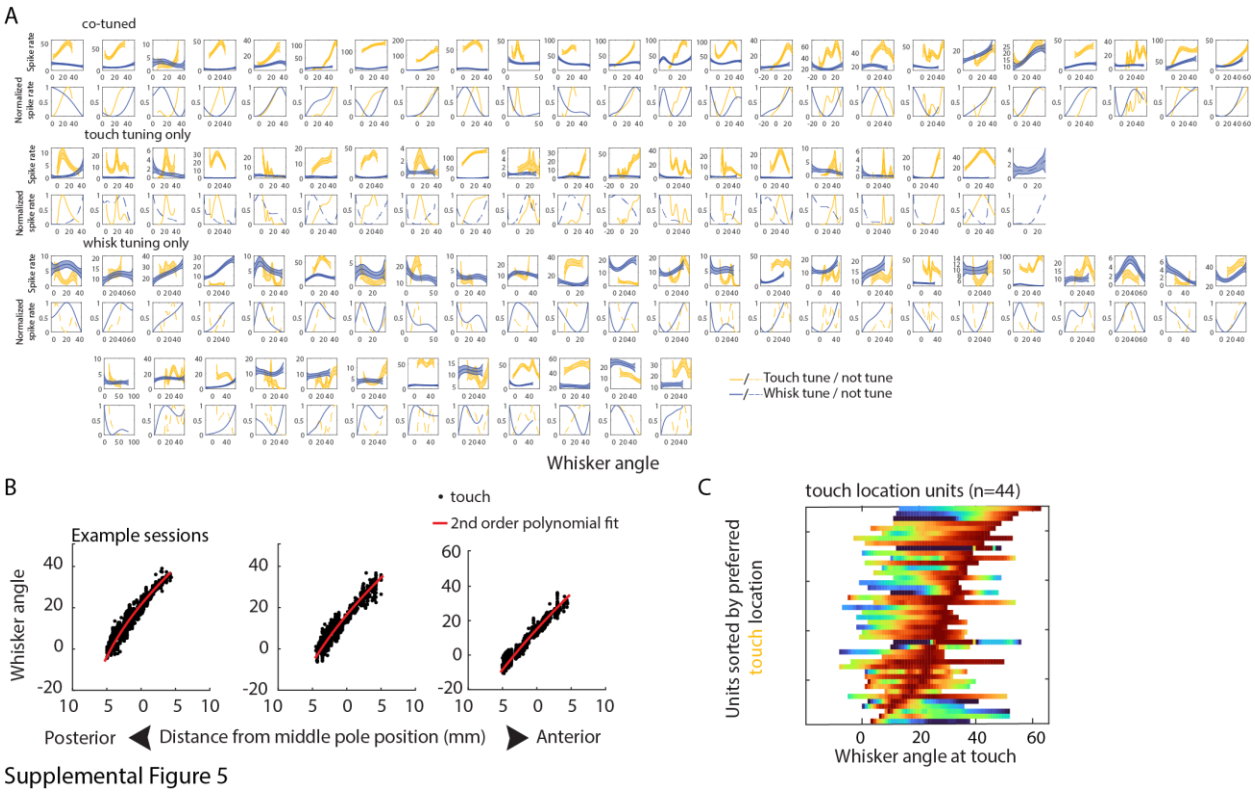

Supplemental Figure 5

Supplementary figure 5 Co-tuning of whisker angle during free-whisking and touch

A) Tuning curves with observed firing rates (top) and normalized firing rates (bottom) for co-tuned (n=25), touch tuned only (n=19), and whisking tuned only units (n=36). Solid lines and dashed lines denote tuning and not tuning respectively. B) Whisker angle at touch is tightly correlated with anteroposterior object location. Three example sessions are shown. C) Population heat map of angle tuned units, sorted by preferred angle at touch. White spaces are insufficiently sampled pole locations.

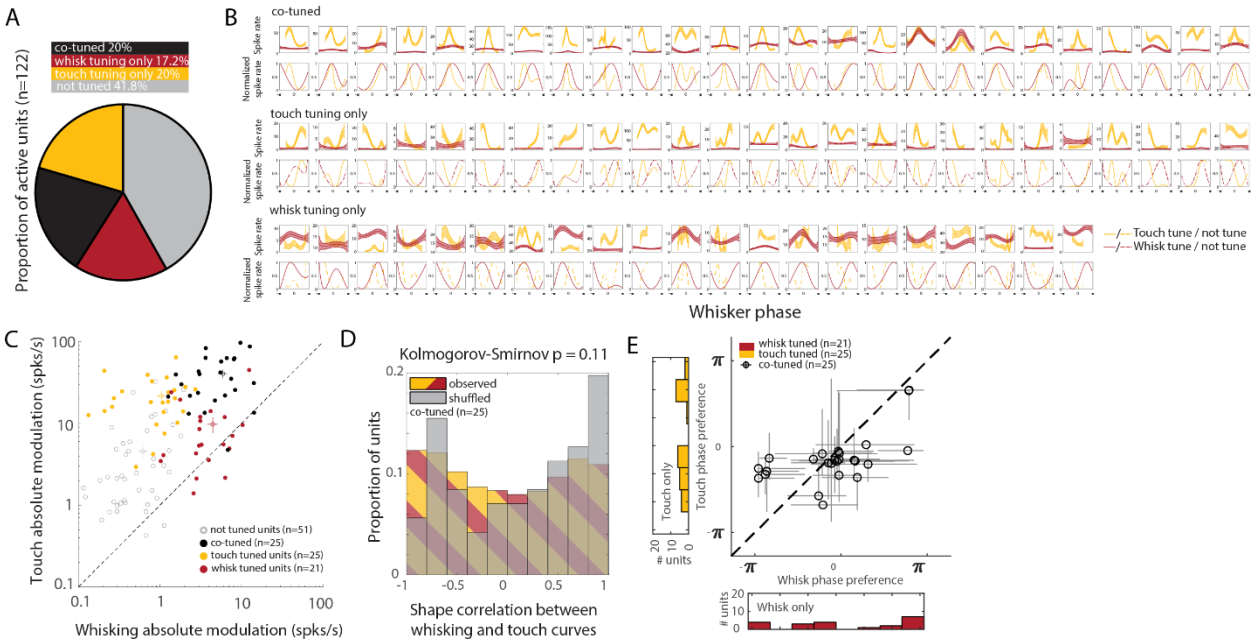

Supplemental Figure 6

Supplementary figure 6 Co-tuning of whisker phase during free-whisking and touch

A) Pie chart highlighting proportion of units phase tuned (maroon, 21/122), at touch (gold, 25/122), co-tuned (black, 25/122), or not-tuned (gray, 51/122). B) Tuning curves with observed firing rates (top) and normalized firing rates (bottom) for co-tuned (n=25), touch tuned only (n=25), and whisking tuned only units (n=21). Solid lines and dashed lines denote tuning and not tuning respectively. C) Absolute modulation depth for angle tuning during free-whisking and touch for each class in A. Average absolute modulation depth was 8x greater for touch (16.4 ± 1.8 Hz; mean ± SEM) than for whisking (2.5 ± 0.4 Hz; mean ± SEM) D) Shape correlation between whisking and touch tuning curves for all units tuned to whisking and/or touch (maroon and gold hash) compared to shuffled responses (gray). Kolmogorov-Smirnov p=0.11. E) Scatter of preference during free-whisking and touch for co-tuned units (mean ± SD; 0.7 ± 0.5 radians, p = 4.6e-7, *t*-stat = 6.8, df = 24; one sample *t*-test). Histograms denote phase preference for units tuned to either touch or free-whisking phase.

REFERENCES

1. Francis, B. A., & Wonham, W. M. (1976). The internal model principle of control theory. Automatica, *12*(5), 457-465.
2. Wolpert, D. M., Ghahramani, Z., & Jordan, M. I. (1995). An internal model for sensorimotor integration. Science, *269*(5232), 1880-1882.
3. Vincent, S. B. (1912). The function of vibrissae in the behavior of the white rat. Behavior Monographs *1*(5): 1-82.
4. Sofroniew, N. J., Vlasov, Y. A., Hires, S. A., Freeman, J., & Svoboda, K. (2015). Neural coding in barrel cortex during whisker-guided locomotion. Elife, *4*, e12559.
5. Høydal, Ø. A., Skytøen, E. R., Andersson, S. O., Moser, M. B., & Moser, E. I. (2019). Object-vector coding in the medial entorhinal cortex. Nature, *568*(7752), 400-404.
6. Lederman, S. J., & Klatzky, R. L. (1987). Hand movements: A window into haptic object recognition. *Cognitive psychology*, *19*(3), 342-368.
7. Knutsen, P.M., Pietr, M. and Ahissar, E. (2006). Haptic object localization in the vibrissal system: behavior and performance. Journal of Neuroscience *26*(33), 8451-8464.
8. Mehta, S. B., Whitmer, D., Figueroa, R., Williams, B. A., & Kleinfeld, D. (2007). Active spatial perception in the vibrissa scanning sensorimotor system. PLoS biology, *5*(2).
9. Horev, G., Saig, A., Knutsen, P. M., Pietr, M., Yu, C., & Ahissar, E. (2011). Motor–sensory convergence in object localization: a comparative study in rats and humans. Philosophical Transactions of the Royal Society B: Biological Sciences, *366*(1581), 3070-3076.
10. Cheung, J., Maire, P., Kim, J., Sy, J. and Hires, S.A., (2019). The sensorimotor basis of whisker-guided anteroposterior object localization in head-fixed mice. Current Biology, *29*(18), 3029-3040.
11. Li, L., Rutlin, M., Abraira, V.E., Cassidy, C., Kus, L., Gong, S., Jankowski, M.P., Luo, W., Heintz, N., Koerber, H.R. and Woodbury, C.J., (2011). The functional organization of cutaneous low-threshold mechanosensory neurons. Cell, *147*(7), pp.1615-1627.
12. Severson, K. S., Xu, D., Van de Loo, M., Bai, L., Ginty, D. D., & O'Connor, D. H. (2017). Active touch and self-motion encoding by merkel cell-associated afferents. Neuron, *94*(3), 666-676.
13. Furuta, T., Bush, N.E., Yang, A.E.T., Ebara, S., Miyazaki, N., Murata, K., Hirai, D., Shibata, K.I. and Hartmann, M.J., 2020. The Cellular and Mechanical Basis for Response Characteristics of Identified Primary Afferents in the Rat Vibrissal System. Current Biology.
14. Jadhav, S. P., Wolfe, J., & Feldman, D. E. (2009). Sparse temporal coding of elementary tactile features during active whisker sensation. Nature neuroscience, *12*(6), 792
15. Isett, B. R., Feasel, S. H., Lane, M. A., & Feldman, D. E. (2018). Slip-based coding of local shape and texture in mouse S1. Neuron, *97*(2), 418-433.
16. Zuo, Y., & Diamond, M. E. (2019). Texture identification by bounded integration of sensory cortical signals. Current Biology, *29*(9), 1425-1435.
17. Chan, T. C., & Turvey, M. T. (1991). Perceiving the vertical distances of surfaces by means of a hand-held probe. Journal of experimental psychology: Human perception and performance, *17*(2), 347.
18. Miller, L.E., Fabio, C., Ravenda, V., Bahmad, S., Koun, E., Salemme, R., Luauté, J., Bolognini, N., Hayward, V. and Farnè, A., (2019). Somatosensory cortex efficiently processes touch located beyond the body. Current Biology.
19. Knutsen, P.M., Biess, A., and Ahissar, E. (2008). Vibrissal kinematics in 3D: tight coupling of azimuth, elevation, and torsion across different whisking modes. Neuron *59*(1), 35-42.
20. Clack, N.G., O'Connor, D.H., Huber, D., Petreanu, L., Hires, A., Peron, S., Svoboda, K. and Myers, E.W. (2012). Automated tracking of whiskers in videos of head fixed rodents. PLoS computational biology *8*(7), e1002591.

21. Hires, S. A., Pammer, L., Svoboda, K., and Golomb, D. (2013). Tapered whiskers are required for active tactile sensation. Elife *2*, e01350.
22. Pammer, L., O'Connor, D. H., Hires, S. A., Clack, N. G., Huber, D., Myers, E. W., and Svoboda, K. (2013). The mechanical variables underlying object localization along the axis of the whisker. Journal of Neuroscience *33*(16), 6726-6741.
23. Hires, S. A., Schuyler, A., Sy, J., Huang, V., Wyche, I., Wang, X., & Golomb, D. (2016). Beyond cones: an improved model of whisker bending based on measured mechanics and tapering. Journal of neurophysiology, 116(2), 812-824.
24. Vaxenburg R., Wyche I., Svoboda K., Efros A. L., and Hires S. A. (2018). Dynamic cues for whisker-based object localization: An analytical solution to vibration during active whisker touch. PLoS Comput Biol. *14*(3)
25. Woolsey, T. A., & Van der Loos, H. (1970). The structural organization of layer IV in the somatosensory region (SI) of mouse cerebral cortex: the description of a cortical field composed of discrete cytoarchitectonic units. Brain research, *17*(2), 205-242.
26. Masino, S. A., Kwon, M. C., Dory, Y., & Frostig, R. D. (1993). Characterization of functional organization within rat barrel cortex using intrinsic signal optical imaging through a thinned skull. Proceedings of the National Academy of Sciences, *90*(21), 9998-10002.
27. O'Connor, D. H., Clack, N. G., Huber, D., Komiyama, T., Myers, E. W., & Svoboda, K. (2010). Vibrissa-based object localization in head-fixed mice. Journal of Neuroscience, *30*(5), 1947-1967.
28. Aronoff, R., & Petersen, C. (2008). Layer, column and cell-type specific genetic manipulation in mouse barrel cortex. Frontiers in neuroscience, *2*, 1.
29. Gerfen, C. R., Paletzki, R., & Heintz, N. (2013). GENSAT BAC cre-recombinase driver lines to study the functional organization of cerebral cortical and basal ganglia circuits. Neuron, *80*(6), 1368-1383.
30. Hong, Y. K., Lacefield, C. O., Rodgers, C. C., & Bruno, R. M. (2018). Sensation, movement and learning in the absence of barrel cortex. Nature, *561*(7724), 542.
31. Lévesque, M., Charara, A., Gagnon, S., Parent, A., & Deschênes, M. (1996). Corticostriatal projections from layer V cells in rat are collaterals of long-range corticofugal axons. Brain research, *709*(2), 311-315.
32. Kita, T., & Kita, H. (2012). The subthalamic nucleus is one of multiple innervation sites for long-range corticofugal axons: a single-axon tracing study in the rat. Journal of Neuroscience, *32*(17), 5990-5999.
33. Shepherd, G. M. (2013). Corticostriatal connectivity and its role in disease. Nature Reviews Neuroscience, *14*(4), 278.
34. Kleinfeld, D., & Deschênes, M. (2011). Neuronal basis for object location in the vibrissa scanning sensorimotor system. Neuron, *72*(3), 455-468.
35. Armstrong-James, M., Fox, K., & Das-Gupta, A. (1992). Flow of excitation within rat barrel cortex on striking a single vibrissa. Journal of neurophysiology, *68*(4), 1345-1358.
36. Fee, M. S., Mitra, P. P., and Kleinfeld, D. (1997). Central versus peripheral determinants of patterned spike activity in rat vibrissa cortex during whisking. Journal of neurophysiology, *78*(2) 1144-1149.
37. De Kock, C. P. J., Bruno, R. M., Spors, H., & Sakmann, B. (2007). Layer-and cell-type-specific suprathreshold stimulus representation in rat primary somatosensory cortex. The Journal of physiology, *581*(1), 139-154.
38. Petreanu, L., Mao, T., Sternson, S.M., and Svoboda, K. (2009). The subcellular organization of neocortical excitatory connections. Nature *457*(7233), 1142.
39. Hires, S. A., Gutnisky, D. A., Yu, J., O'Connor, D. H., and Svoboda, K. (2015). Low-noise encoding of active touch by layer 4 in the somatosensory cortex. Elife *4*, e06619.
40. Hill, D. N., Curtis, J. C., Moore, J. D., and Kleinfeld, D. (2011). Primary motor cortex reports efferent control of vibrissa motion on multiple timescales. Neuron *72*(2), 344-356.

41. Petreanu, L., Gutnisky, D.A., Huber, D., Xu, N.L., O'Connor, D.H., Tian, L., Looger, L., and Svoboda, K. (2012). Activity in motor–sensory projections reveals distributed coding in somatosensation. Nature *489*(7415), 299.
42. Xu, N. L., Harnett, M. T., Williams, S. R., Huber, D., O'connor, D. H., Svoboda, K., and Magee, J. C. (2012). Nonlinear dendritic integration of sensory and motor input during an active sensing task. Nature *492*(7428), 247.
43. Ranganathan, G.N., Apostolides, P.F., Harnett, M.T., Xu, N.L., Druckmann, S., and Magee, J.C. (2018). Active dendritic integration and mixed neocortical network representations during an adaptive sensing behavior. Nature neuroscience *21*(11), 1583-1590.
44. Curtis, J.C., and Kleinfeld, D. (2009). Phase-to-rate transformations encode touch in cortical neurons of a scanning sensorimotor system. Nat. Neurosci. *12*, 492–501.
45. Lefort, S., Tomm, C., Sarria, J. C. F., & Petersen, C. C. (2009). The excitatory neuronal network of the C2 barrel column in mouse primary somatosensory cortex. Neuron, *61*(2), 301-316.
46. O'connor DH, Peron SP, Huber D, Svoboda K. Neural activity in barrel cortex underlying vibrissa-based object localization in mice. Neuron. 2010;67(6):1048-61.
47. Pégard, N. C., Mardinly, A. R., Oldenburg, I. A., Sridharan, S., Waller, L., & Adesnik, H. (2017). Three-dimensional scanless holographic optogenetics with temporal focusing (3D-SHOT). Nature communications, *8*(1), 1228.
48. Marshel, J.H., Kim, Y.S., Machado, T.A., Quirin, S., Benson, B., Kadmon, J., Raja, C., Chibukhchyan, A., Ramakrishnan, C., Inoue, M. and Shane, J.C., (2019). Cortical layer–specific critical dynamics triggering perception. Science, *365*(6453), p.eaaw5202.
49. De Kock, C. P. J., & Sakmann, B. (2008). High frequency action potential bursts (≥ 100 Hz) in L2/3 and L5B thick tufted neurons in anaesthetized and awake rat primary somatosensory cortex. The Journal of *physiology*, *586*(14), 3353-3364.
50. Huang, L., Knoblich, U., Ledochowitsch, P., Lecoq, J., Reid, R.C., de Vries, S.E., Buice, M.A., Murphy, G.J., Waters, J., Koch, C. and Zeng, H., (2019). Relationship between spiking activity and simultaneously recorded fluorescence signals in transgenic mice expressing GCaMP6. bioRxiv, p.788802.
51. Yu, J., Gutnisky, D. A., Hires, S. A., & Svoboda, K. (2016). Layer 4 fast-spiking interneurons filter thalamoco drtical signals during active somatosensation. Nature neuroscience, *19*(12), 1647.
52. Peron, S. P., Freeman, J., Iyer, V., Guo, C., & Svoboda, K. (2015). A cellular resolution map of barrel cortex activity during tactile behavior. Neuron, *86*(3), 783-799.
53. Hooks, B.M., Hires, S.A., Zhang, Y.X., Huber, D., Petreanu, L., Svoboda, K., and Shepherd, G.M. (2011). Laminar analysis of excitatory local circuits in vibrissal motor and sensory cortical areas. PLoS biology *9*(1), e1000572.
54. Larkum, M. E., Zhu, J. J., & Sakmann, B. (1999). A new cellular mechanism for coupling inputs arriving at different cortical layers. *Nature*, *398*(6725), 338.
55. Guo, Z.V., Hires, S.A., Li, N., O'Connor, D.H., Komiyama, T., Ophir, E., Huber, D., Bonardi, C., Morandell, K., Gutnisky, D. and Peron, S., 2014. Procedures for behavioral experiments in head-fixed mice. PloS one, 9(2).
56. Wallstrom, G., Liebner, J., & Kass, R. E. (2008). An implementation of Bayesian adaptive regression splines (BARS) in C with S and R wrappers. Journal of Statistical Software, *26*(1), 1.
57. Hastie, T., & Qian, J. (2014). Glmnet vignette. *Retrieve from http://www. web. stanford. edu/~ hastie/Papers/Glmnet_Vignette. pdf. Accessed September*, *20*, 2016.